JCI The Journal of Clinical Investigation

Purinergic P2X4 receptors and mitochondrial ATP production regulate T cell migration

Carola Ledderose, Kaifeng Liu, Yutaka Kondo, Christian J. Slubowski, Thomas Dertnig, Sara Denicoló, Mona Arbab, Johannes Hubner, Kirstin Konrad, Mahtab Fakhari, James A. Lederer, Simon C. Robson, Gary A. Visner, Wolfgang G. Junger

J Clin Invest. 2018. https://doi.org/10.1172/JCI120972.

Research Article In-Press Preview **Cell biology**

T cells must migrate in order to encounter antigen-presenting cells (APCs) and to execute their varied functions in immune defense and inflammation. ATP release and autocrine signaling through purinergic receptors contribute to T cell activation at the immune synapse that T cells form with APCs. Here, we show that T cells also require ATP release and purinergic signaling for their migration to APCs. We found that the chemokine SDF-1α triggered mitochondrial ATP production, rapid bursts of ATP release, and increased migration of primary human $CD4^+$ T cells. This process depended on pannexin-1 ATP release channels and autocrine stimulation of P2X4 receptors. SDF-1α stimulation caused localized accumulation of mitochondria with P2X4 receptors near the front of cells, resulting in a feed-forward signaling mechanism that promotes cellular Ca^{2+} influx and sustains mitochondrial ATP synthesis at levels needed for pseudopod protrusion, T cell polarization, and cell migration. Inhibition of P2X4 receptors blocked the activation and migration of T cells in vitro. In a mouse lung transplant model, P2X4 receptor antagonist treatment prevented the recruitment of T cells into allograft tissue and the rejection of lung transplants. Our findings suggest that P2X4 receptors are therapeutic targets for immunomodulation in transplantation and inflammatory diseases.

Purinergic P2X4 receptors and mitochondrial ATP production regulate T cell migration

Carola Ledderose[1], Kaifeng Liu[2], Yutaka Kondo[1], Christian J. Slubowski[1], Thomas Dertnig[1], Sara Denicoló[1], Mona Arbab[1], Johannes Hubner[1], Kirstin Konrad[1], Mahtab Fakhari[1], James A. Lederer[3], Simon C. Robson[4], Gary A. Visner[2], Wolfgang G. Junger[1,5]

[1]Department of Surgery, Beth Israel Deaconess Medical Center, Harvard Medical School, Boston, Massachusetts, USA; [2]Department of Medicine/Pediatrics, Boston Children's Hospital, Harvard Medical School, Boston, Massachusetts, USA; [3]Department of Surgery, Brigham and Women's Hospital, Harvard Medical School, Boston, Massachusetts, USA; [4]Department of Medicine, Beth Israel Deaconess Medical Center, Harvard Medical School, Boston, Massachusetts, USA; [5]Ludwig Boltzmann Institute for Traumatology, Vienna, Austria

*Correspondence address: Wolfgang G. Junger, Harvard Medical School, Beth Israel Deaconess Medical Center, Department of Surgery, 330 Brookline Avenue, Boston, MA 02215, USA; phone: (617) 667-7415, Fax: (617) 667-7419; e-mail: wjunger@bidmc.harvard.edu

ABSTRACT

T cells must migrate in order to encounter antigen-presenting cells (APCs) and to execute their varied functions in immune defense and inflammation. ATP release and autocrine signaling through purinergic receptors contribute to T cell activation at the immune synapse that T cells form with APCs. Here, we show that T cells also require ATP release and purinergic signaling for their migration to APCs. We found that the chemokine SDF-1α triggered mitochondrial ATP production, rapid bursts of ATP release, and increased migration of primary human $CD4^+$ T cells. This process depended on pannexin-1 ATP release channels and autocrine stimulation of P2X4 receptors. SDF-1α stimulation caused localized accumulation of mitochondria with P2X4 receptors near the front of cells, resulting in a feed-forward signaling mechanism that promotes cellular Ca^{2+} influx and sustains mitochondrial ATP synthesis at levels needed for pseudopod protrusion, T cell polarization, and cell migration. Inhibition of P2X4 receptors blocked the activation and migration of T cells in vitro. In a mouse lung transplant model, P2X4 receptor antagonist treatment prevented the recruitment of T cells into allograft tissue and the rejection of lung transplants. Our findings suggest that P2X4 receptors are therapeutic targets for immunomodulation in transplantation and inflammatory diseases.

INTRODUCTION

T cells have important roles in host immune defense and inflammation. These involve the migration of T cells into secondary lymphoid organs where they search for matching antigens that are displayed by antigen-presenting cells (APCs). In lymph nodes, cell migration enables T cells to sequentially interrogate APCs for cognate antigens capable of causing T cell activation (1-3). The mechanisms that regulate T cell migration are only partially understood (4, 5). An in-depth understanding of these mechanisms may lead to the development of novel therapeutic strategies to modulate host immune defenses and to prevent the recruitment of T cells into inflamed tissues that are damaged in the course of allergic and autoimmune diseases such as Crohn's disease, rheumatoid arthritis, lupus erythematosus, and multiple sclerosis (6, 7). T cells that infiltrate donor tissues following organ transplantation cause cellular rejection, which is a particularly serious and unresolved problem in lung transplantation (8, 9).

A large number of chemokines and their corresponding receptors regulate T cell trafficking into target tissues (10). One of these chemokines is stromal-derived factor-1α (SDF-1α, also known as CXCL12) that binds to the chemokine receptor CXCR4 and contributes to the homing of $CD4^+$ T cells into secondary lymphoid organs and regulates cell migration within lymph nodes (11-13). SDF-1α also causes T cell recruitment to the lungs in allergic airway diseases and into lung allografts (14, 15). Here we show that SDF-1α triggers the activation of mitochondrial ATP production and the release of cellular ATP from naïve T cells. It is well known that extracellular ATP and purinergic signaling play important roles in the regulation of immunity and inflammation (16-18). Others and we have shown that cellular ATP release and autocrine stimulation of P2X1, P2X4, and P2X7 receptors regulate T cell receptor (TCR) signaling, enhance IL-2 production, and induce the proliferation of T cells (19-21). Here we show that ATP release into the pericellular space is also essential for T cell migration, namely by fueling autocrine signaling via P2X4 receptors that regulate pseudopod protrusion and the migration of T cells in response to SDF-1α. We found that pharmacological targeting of P2X4 receptors prevents T cell migration and the recruitment of T cells into lung allograft tissue in a mouse lung transplant model, suggesting that P2X4 receptor signaling is a therapeutic target to prevent organ rejection.

RESULTS

SDF-1α triggers rapid ATP release and T cell migration

Cell migration is a fundamental feature by which T cells traffic to lymph nodes and other tissues to scan APCs for suitable antigens (4). Over a dozen different chemokine receptors regulate T cell trafficking (10). CXCR4 and its ligand SDF-1α are involved in the recruitment of lymphocytes to lymph nodes and allograft tissues (11, 14, 15). T cell trafficking into transplanted lungs leads to graft rejection, which is an unresolved problem that limits success in lung transplantation (9, 22). A better understanding of the mechanisms that regulate T cell migration may reveal novel therapeutic targets to prevent allograft rejection. We found that SDF-1α stimulation of naïve $CD4^+$ T cells induces rapid cell polarization, robust migration, and the release of cellular ATP (Figure 1, A and B; Supplemental Figure 1A, Supplemental Video 1). SDF-1α dose-dependently increased migration speed and the area covered by T cells (Figure 1C). Studies with a novel membrane-anchoring ATP probe, 2-2Zn (23, 24), revealed that SDF-1α triggers a sudden surge of ATP release within seconds of cell stimulation (Figure 1, A and D; Supplemental Video 2). SDF-1α-induced ATP release was blocked by the gap junction inhibitor carbenoxolone (CBX) and the pannexin 1 (PANX1) channel inhibitor ^{10}panx1 (Figure 1, D and E; Supplemental Video 2). Next, we examined the role of PANX1 in the migration of Jurkat cells, a $CD4^+$ T cell line that is often used to study $CD4^+$ T cell activation mechanisms and that reacted similarly to SDF1-a stimulation (Supplemental Figure 1). Silencing of PANX1 channels in Jurkat cells blocked SDF-1α-induced ATP release, polarization, and cell migration (Figure 1F; Supplemental Video 3). These findings and similar recent reports by others demonstrate that ATP release via PANX1 channels is required for the migration of $CD4^+$ T cells in response to SDF-1α (25).

Mitochondria produce the ATP that regulates T cell migration

In our previous work, we have shown that mitochondria fuel autocrine purinergic feedback mechanisms that maintain basal functions of resting T cells (26). In activated T cells, a burst of mitochondrial activity promotes T cell receptor signaling at the immune synapse between T cells and APCs (27). Here, we show that mitochondria also regulate cell migration. Inhibition of mitochondria by uncoupling oxidative phosphorylation with carbonyl cyanide m-chlorophenyl hydrazine (CCCP) blocked ATP release and the polarization and migration of T cells in response to SDF-1α (Figure 2, A-C). Blocking ATP release or inhibition of P2 receptor stimulation by treating cells with CBX, suramin, or by removing released ATP with apyrase impaired the polarization and migration of cells in response to SDF-1α (Figure 2, B and C). Thus, SDF-1α-induced mitochondrial ATP production fuels autocrine feedback mechanisms that regulate $CD4^+$

T cell migration. In order to study how SDF-1α elicits ATP production, we used Rhod-2 to assess Ca^{2+} uptake by mitochondria, which is a prerequisite for mitochondrial ATP synthesis (28). Using live-cell imaging with Rhod-2 and 2-2Zn, we found that mitochondrial Ca^{2+} uptake and hotspots of ATP release coincided with sites of pseudopod protrusion and membrane remodeling (Figure 2, D and E; Supplemental Video 4). These findings suggest that SDF-1α triggers mitochondrial activation and localized ATP release that regulates pseudopod protrusion at the front of migrating T cells.

P2X4 receptors regulate T cell migration

SDF-1α dose-dependently increased the activation of T cells in PBMC cultures stimulated under conditions that necessitate T cell migration for the ligation of both the TCR and CD28 co-receptor (Figure 3A). Adding SDF-1α to PBMC cultures stimulated with soluble anti-CD3 antibodies in flat-bottom dishes increased the migration speed of T cells, the range the cells covered, and the expression of CD69 that was assessed as an early T cell activation event (Figure 3B; Supplemental Figure 2A). There was a positive correlation between parameters of cell migration (migration speed or range) and cell activation (CD69 expression; Figure 3C; Supplemental Figure 2B). While SDF-1α increased cell migration, it did not alter coupling of T cells with anti-TCR/CD28 antibody-coated beads (Supplemental Figure 2, C and D). This suggests that ATP release in response to SDF-1α and autocrine stimulation of purinergic receptors promotes T cell activation by increasing cell migration, the rate of T cell/APC encounters, and the formation of immune synapses. Of the 19 known mammalian purinergic receptor subtypes, which comprise four P1 (adenosine), seven P2X, and eight P2Y receptors, all seven ionotropic P2X receptors and several of the G-protein coupled P2Y ($P2Y_2$, $P2Y_{11}$, $P2Y_{13}$) receptor subtypes are capable of recognizing ATP (29-31). Of these ATP receptors, $CD4^+$ T cells express the P2X1, P2X4, P2X7, and $P2Y_{11}$ receptor subtypes (20, 32). The P2X1, P2X4, and P2X7 subtypes contribute to immune synapse signaling, but the role of these receptors in T cell migration is not known (20). We found that 5-(3-Bromophenyl)-1,3-dihydro-2*H*-benzofuro[3,2-*e*]-1,4-diazepin-2-one (5-BDBD), a specific and selective P2X4 receptor antagonist (33-35), impaired T cell migration in response to SDF-1α (Figure 3D). Inhibition of P2X1 or P2X7 receptors with NF023 and A438079, respectively, had less effect on cell migration. Inhibition of P2X4 receptors was also more effective than inhibition of P2X1 or P2X7 receptors in suppressing CD69 expression and the proliferation of $CD4^+$ T cells (Figure 3, E and F; Supplemental Figure 3). Taken together, these findings show that P2X4 receptor signaling has a special role in the regulation of T cell migration.

P2X4 receptors modulate cytosolic and mitochondrial Ca^{2+} levels in response to SDF-1α

P2X4 receptors act as ATP-gated Ca^{2+} channels that facilitate Ca^{2+} influx, which is required for mitochondrial activity (28, 30). Therefore, we studied the role of P2X4 receptors in SDF-1α-induced Ca^{2+} signaling. The P2X4 receptor antagonist 5-BDBD reduced cytosolic Ca^{2+} signaling and completely abolished mitochondrial Ca^{2+} uptake and cellular ATP release in response to SDF-1α (Figure 4, A-E; Supplemental Video 5). These findings suggest that endogenous P2X4 receptor stimulation promotes a feed-forward signaling mechanism that upregulates mitochondrial ATP production in response to SDF-1α. This is supported by the finding that blocking ATP release with CBX and inhibition of P2X4 receptors had similar effects on SDF-1α-induced Ca^{2+} signaling. CXCR4 stimulation is known to activate phosphatidylinositol 3-kinase (PI3K) signaling, which promotes the release of Ca^{2+} from intracellular stores (36). Treatment with the selective PI3K inhibitor wortmannin prevented the increase in intracellular Ca^{2+} following SDF-1α stimulation, which suggests that P2X4 receptors enhance and sustain mitochondrial activity following SDF-1α exposure (Figure 4, A-D).

P2X4 receptors are needed for T cell polarization and pseudopod formation

Leukocyte migration depends on the polarization of cells, which involves excitatory signals that promote actin polymerization and pseudopod protrusion at the leading edge (37). We hypothesized that P2X4 receptors provide such signals to enhance and amplify chemokine signaling and establish cell polarity in migrating T cells. We found that silencing of P2X4 receptors disrupts cell polarization and the migration of T cells in response to SDF-1α (Figure 5, A-C; Supplemental Video 6). In the absence of P2X4 receptor signaling, T cells assumed rounded shapes with a reduced cell surface area (Figure 5, A and D) and fewer pseudopodia (Figure 5E). Upon TCR stimulation, T cells transform into spontaneously migrating lymphoblasts that require P2X4 receptors for cell migration as shown by the fact that 5-BDBD dose-dependently and reversibly blocked the polarization and migration of TCR/CD28-stimulated T cells (Supplemental Figure 4; Figure 5; Supplemental Video 6).

P2X4 receptors regulate mitochondrial ATP production in migrating T cells

In order to study the role of P2X4 receptors in cell migration, we examined the subcellular distribution of P2X4 receptors using fluorescence-tagged P2X4 receptor fusion proteins expressed in Jurkat $CD4^+$ T cells. In unstimulated cells, P2X4 receptors were expressed in punctae that were distributed throughout the plasma membrane. Cell stimulation and polarization resulted in a reorganized pattern with these P2X4 receptor containing structures located primarily at the front of polarized cells. P2X4 receptors accumulated at sites of

pseudopod protrusion that also featured increased mitochondrial activity (Figure 6A; Supplemental Video 7). Like others before, we also observed that active mitochondria frequently accumulate near the uropod of migrating cells where they are thought to fuel ATP consuming actin-myosin-driven cell contraction (Figure 6B) (38). We found that cell migration speed correlated with the proportion of mitochondrial mass near the uropod (Figure 6C; Supplemental Figure 5A). Slow-moving cells, however, used a portion of their mitochondria at the front to probe the extracellular environment and to communicate with adjacent cells using their pseudopodia (Figure 6, B and D; Supplemental Video 8). These findings indicate that the subcellular distribution of mitochondria determines patterns of cell motility and behavior. The accumulation of mitochondria and P2X4 receptors near the leading edge of migrating cells suggests that their tight interaction is required to promote excitatory signaling mechanisms that facilitate pseudopod protrusion. In support of this notion, we found that inhibition of P2X4 receptors resulted in a progressive shutdown of mitochondrial activity and the retraction of lamellipodia (Figure 6, E and F; Supplemental Video 9). Removal of extracellular ATP by apyrase had a similar effect, which is in agreement with an autocrine purinergic feed-forward signaling loop that regulates mitochondrial activity (Figure 6F). Taken together, these findings demonstrate that the subcellular localization of P2X4 receptors and of the mitochondria that fuel these receptors has a central role in the regulation of T cell polarization and migration. This conclusion is further supported by our findings that the mitochondrial inhibitors CCCP, rotenone, and oligomycin impaired cell polarization, pseudopod formation, and cell migration (Supplemental Figure 5, B-E).

P2X4 receptor inhibition prevents T cell infiltration and lung allograft rejection

Cell migration is needed for the recruitment of alloreactive T cells into lung allograft tissues, where these cells cause acute and chronic transplant rejection (22). We tested whether pharmacological inhibition of P2X4 receptors prevents the infiltration of T cells into lung allografts using a mouse lung transplant model with major histocompatibility complex mismatched BALB/c (H-2^d) donor lungs and C57BL/6 (H-2^b) recipient mice. We chose this widely used model because it recapitulates the clinical situation where human leukocyte antigen (HLA) mismatches are unavoidable due to logistic constraints (39, 40). We determined T cell recruitment into the lung allograft 24 h after lung transplantation, i.e., at a time early enough to exclude the possibility that T cell proliferation interfered with cell numbers in allograft tissues. Treatment with the P2X4 receptor antagonist 5-BDBD reduced the accumulation of T cells in lung allografts, improved lung function as reflected in reduced peak airway pressures and reduced the gross appearance of rejection when compared to allografts implanted into vehicle-

treated control mice (Figure 7, A and B; Supplemental Figure 6). Moreover, P2X4 receptor inhibition also blocked the proliferation of $CD4^+$ and $CD8^+$ C57BL/6 recipient T cells in mixed lymphocyte reactions with BALB/c donor splenocytes (Figure 7, C and D; Supplemental Figure 6). The effect of suramin on mouse cells was less effective than its effect on human cells (Figure 3F). This may be due to species differences that have been previously reported for this inhibitor (41). Taken together, these data demonstrate that blocking P2X4 receptors can indeed prevent the recruitment and activation of alloreactive T cells in lung transplantation.

DISCUSSION

T cell migration is an important but only partially understood lymphocyte function (2, 4, 5). In our previous work, we have shown that autocrine purinergic signaling mechanisms fine-tune the directed migration of neutrophils in a chemotactic gradient field (42-44). Chemotaxis is essential for neutrophils to pursue and eliminate invading microbes. T cells require a more complex repertoire of motility patterns to fulfill their diverse roles in host immune defense (3, 45). Several mathematical models have been developed to describe different migration modes such as Brownian motion, random walk, and Levy walk (4, 46, 47). However, the underlying molecular mechanisms that orchestrate these different migration patterns are incompletely understood.

SDF-1α is one of the chemokines involved in the migration of T cells in lung allotransplants and lymph nodes (11, 15, 48). We found that stimulation of the corresponding chemokine receptor, CXCR4, triggers rapid ATP release from $CD4^+$ T cells and that the released ATP regulates T cell migration through autocrine stimulation of P2X4 receptors. Recently, we have shown that naïve $CD4^+$ T cells rely on basal autocrine purinergic signaling to maintain cell metabolism in a “stand-by” mode that is needed for immune surveillance (26). Release of low amounts of ATP from resting cells is sufficient to stimulate high-affinity P2X1 receptors that promote Ca^{2+} influx and maintain basal mitochondrial activity at levels needed for immune surveillance. Here we show that SDF-1α increases ATP release to the levels needed to stimulate P2X4 receptors that promote the transition of cells from the resting state to a “search mode”. Our results suggest that the localization of mitochondria is a key determinant of cell polarization, pseudopod formation, and cell migration. Mitochondrial accumulation near the uropod of migrating leukocytes has been reported before and may provide the ATP needed for cell migration (38). We found that translocation of a portion of the mitochondrial mass to the front allows cells to probe their environment in order to interact with other cells. Our findings suggest that mitochondria at the front are needed to fuel autocrine purinergic signaling through P2X4 receptors. Further studies

will be needed to determine the mechanisms that regulate the distribution of mitochondria in polarized and migrating T cells and to distinguish these mechanisms from other effects such as passive displacement by the nucleus.

Based on our findings, we propose the following mechanisms by which excitatory P2X4 receptors regulate T cell migration (Figure 7E): Stimulation of chemokine receptors, e.g., with SDF-1α, triggers downstream signaling that activates mitochondrial ATP production and ATP release through PANX1 channels. P2X4 receptors co-localize with mitochondria in clusters at the front of cells and facilitate Ca^{2+} influx to maintain local mitochondrial ATP production at the levels needed for cell migration. P2X4 receptor-induced Ca^{2+} signaling may also promote cytoskeletal remodeling that is required for cell migration, TCR signaling, and immune synapse formation (49, 50). Cell migration and immune synapse formation lead to the clustering of active mitochondria with PANX1 channels and P2X1 and P2X4 receptors, which elicits a final boost of localized ATP release that leads to full-fletched T cell effector functions (19, 20, 27).

Targeting T cell migration can prevent the influx of T cells into inflamed tissues and T cell activation in transplanted organs, which leads to pathological inflammatory responses, including allograft rejection. The potential of targeting chemokine receptors to attenuate allograft rejection has been explored before but targeting of a single chemokine has shown to yield only marginal improvement (51). Our findings suggest that targeting P2X4 receptors that regulate T cell migration is a more effective strategy to attenuate T cell infiltration into allograft tissues. Inhibition of P2X4 receptor signaling can also block T cell proliferation. Therefore, additional experiments will be necessary to determine potential side effects of long-term treatment with P2X4 receptor antagonists.

P2X4 receptors and related purinergic mechanisms involved in T cell migration may be promising therapeutic targets in lung transplantation as suggested by previous work showing that P2X receptor antagonists could dramatically improve long-term graft survival in a mouse lung transplant model (52). Future studies will be needed to evaluate the pharmacokinetics of 5-BDBD, to refine currently used drug regimens (53, 54), and to study the efficacy of this and future P2X4 receptor antagonists in the prevention of chronic lung allograft rejection.
In summary, we conclude that P2X4 receptors are potential targets to modulate inflammatory processes in organ transplantation and in other inflammatory settings, such as in ischemia and reperfusion injury or inflammatory bowel disease.

METHODS

Reagents

Fluo-4 AM, Rhod-2 AM, MitoTracker Red CM-H2Xros, CFSE and CellTrace Far Red were purchased from Molecular Probes (Thermo Fisher Scientific, Waltham, MA). All antibodies used for flow cytometry experiments were primarily fluorochrome conjugated and purchased from Biolegend (San Diego, CA). In particular, the following antibodies were used in this study: FITC anti-human CD69 (FN 50); APC anti-human CD4 (OKT4); FITC anti-mouse CD3 (17A2); PE anti-mouse CD4 (RM4-5); PerCP anti-mouse CD4 (RM4-5); PE anti-mouse CD8a (53-6.7); PerCP anti-mouse CD8 (53-6.7); APC anti-mouse H-2K^{b} (AF6-88.5); anti-mouse CD16/CD32 (2.4G2; BD Pharmingen, Franklin Lakes, NJ); anti-human CD3 (HIT3a; BD Pharmingen); anti-human CD28 (CD28.2, BD Pharmingen). SDF-1α was from R&D Systems (Minneapolis, MN). Suramin, NF023, NF279, 5-BDBD and ^{10}panx1 were from Tocris (R&D Systems). All other reagents were from Sigma-Aldrich (St. Louis, MO) if not otherwise stated.

Cells

Peripheral blood mononuclear cells (PBMCs) and CD4^{+} T cells were isolated from the blood of healthy volunteers, and primary T cells and Jurkat T cells (clone E6-1; ATCC, Manassas, VA) were maintained as described previously (27). T cells were used immediately after isolation or stimulated for 3 days with Dynabeads (Thermo Fisher Scientific) coated with mouse anti-human anti-CD3 and anti-CD28 antibodies at a bead to cell ratio of 1:1.

T cell polarization, pseudopod formation, and cell migration

Cells were placed into fibronectin-coated (40 µg/ml) 8-well glass bottom chamber slides (La-Tek, Rochester, NY) and suspended in cell culture medium. The chambers were placed in a temperature controlled (37°C) stage incubator and maintained in a humidified gas atmosphere at 5% CO_2 and 21% O_2 (Live Cell Instrument, Seoul, Korea). If applicable, cells were treated with inhibitors at the indicated concentrations 10 min prior to imaging. Cell migration in the presence or absence of SDF-1α (100 ng/ml, if not stated otherwise) was tracked by time-lapse microscopy with a Leica DMRI inverted microscope through a 20x objective (NA 0.4; Leica Microsystems, Wetzlar, Germany) capturing 41 sequential images at 45-s intervals. The migration paths of individual cells were determined with ImageJ software (NIH; MTrackJ plugin) and used to calculate migration speed and the area cells covered (migration range) during the observation period. Cell surface area, cell protrusion size and cell polarization, defined as the ratio of cell length to cell width, were determined with ImageJ. Pseudopodia were defined as previously

described, namely as cell protrusions other than the uropod with a surface area of >6 μm^2 (55). The uropod was defined as the longest protrusion at the back of moving cells. Pseudopodia were manually tracked for 30 min using ImageJ software at 45-s intervals; the number of pseudopodia for each individual cell was determined at each time point.

Live-cell imaging of calcium, mitochondria and ATP release

$CD4^+$ T cells were attached to fibronectin-coated glass bottom chamber slides and stained with the cytosolic Ca^{2+} indicator Fluo-4 AM (4 µM, 20 min), the mitochondrial Ca^{2+} indicator Rhod-2 AM (1 µM, 10 min), or with the mitochondrial membrane potential and ROS-sensitive dye MitoTracker Red CM-H2Xros (100 nM, 10 min) in cell culture medium buffered with 20 mM HEPES. To image ATP release at the cell surface, cells were suspended in Hanks' balanced salt solution and stained for 5 min with 500 nM of a cell-surface targeting fluorescent ATP probe (2-2Zn, gift from Dr. Itaru Hamachi, Kyoto University, Kyoto, Japan) (23). Cells were treated with inhibitors as indicated and stimulated with SDF-1α (100 ng/ml). Fluorescence live-cell imaging was performed with an inverted Leica DMI6000B microscope (Leica Microsystems) equipped with a temperature-controlled (37°C) stage incubator (Live Cell Instrument) and a Leica DFC365 FX camera. Fluorescence images were captured through 63x or 100x oil objectives (NA 1.4) using TRITC and FITC filter sets (Leica Microsystems) and LeicaLAS microscope imaging software. Image analysis was done with ImageJ. To assess mitochondrial localization within polarized T cells, bright field and fluorescence image pairs of migrating cells were acquired. The leading and the trailing edges of each cell were determined by analyzing consecutive image sequences. Bright field images were used to determine cell shapes. Fluorescence images were used to determine the distribution of mitochondria in the front and back halves of each cell.

Transfection and P2X4 receptor distribution

Enhanced green fluorescent protein (EGFP)-tagged P2X4 receptor constructs were generated as previously described (20). Jurkat cells were transfected with 10 µg of the EGFP-P2X4 plasmid by electroporation with a Neon Transfection system (Thermo Fisher Scientific) according to the manufacturer's instructions and cultured in RPMI medium supplemented with 10% heat-inactivated fetal calf serum for 5 h. Cells were imaged with the Leica DMI6000B microscope mentioned above. Prior to imaging, EGFP-P2X4 receptor expressing Jurkat cells were co-stained with MitoTracker Red CM-H2Xros (100 nM for 10 min at 37°C) to estimate co-localization of P2X4 receptors with mitochondria.

Silencing of PANX1 and P2X4 receptors

siRNAs targeting and P2X4 receptors were purchased from Ambion (Silencer Select Pre-Designed siRNA, Thermo Fisher Scientific). A non-targeting siRNA (Qiagen, Germantown, MD) was included as a negative control in all experiments. Jurkat cells were transfected with 10 nM (final concentration) of the respective siRNAs with a Neon Transfection System (Thermo Fisher Scientific) and cultured for 48 h as we had found reliable gene knockdown using these conditions (20).

ATP measurements

Freshly isolated $CD4^+$ T cells or Jurkat cells ($5x10^5$, suspended in 150 µl RPMI medium) were incubated for 10 min with CBX, ^{10}panx1, CCCP or 5-BDBD as indicated, stimulated with SDF-1α (100 ng/ml) for the indicated times and placed on ice to stop reactions. The supernatants were collected by centrifugation at 0°C and ATP concentrations determined using a luciferin/luciferase ATP bioluminescence kit (Thermo Fisher Scientific).

CD69 expression and $CD4^+$ T cell proliferation

PBMCs ($1.5x10^5$/well) were placed into flat-bottom fibronectin-coated 96-well cell culture plates and stimulated with SDF-1α (100 ng/ml) and soluble anti-CD3 antibodies (0.25 µg/ml) for 3 h. CD69 expression in $CD4^+$ T cells was measured by flow cytometry (FACScalibur, BD). Inhibitors as indicated were added during the duration of the experiment. Samples stimulated with anti-CD3/anti-CD28 antibody-coated beads, non-stimulated samples and samples that had been depleted from monocytes by plastic adherence served as positive and negative controls. For proliferation studies, PBMCs were stained with CFSE following the manufacturer's instructions and stimulated for 72 h with anti-CD3 antibodies (0.25 µg/ml) in the presence of inhibitors as indicated. $CD4^+$ T cells were identified by forward and side scatter properties and by staining with anti-CD4 antibodies.

Coupling of T cells and antibody-coated beads

Freshly isolated human $CD4^+$ T cells ($1x10^5$) suspended in 200 µl fully supplemented cell culture medium were treated or not (control) with SDF-1α (10-100 ng/ml) for 10 min, mixed with $1x10^5$ anti-CD3/anti-CD28 antibody-coated microbeads, and incubated in 1.5 ml microcentrifuge tubes at 37°C under gentle agitation in a shaking water bath. Coupling of T cells to beads was determined after 15 min using flow cytometry. Beads were identified by their fluorescence and forward and side scatter properties (Supplemental Figure 2C). Control samples were treated

with latrunculin B (10 µg/ml), an inhibitor of actin polymerization and IS formation in T cells (56), to determine passive binding of cells and beads.

Mice

C57BL/6 and BALB/c mice were purchased from Jackson Laboratories (Bar Harbor, ME) and housed in accordance with institutional and NIH guidelines. For all experiments, male mice, aged 8 to 10 weeks and weighing 20-25 g were used.

Mouse orthotopic lung transplantation

Orthotopic left vascularized lung transplants were performed as previously described using BALB/c (H-2^d) as donor and C57BL/6 (H-2^b) as recipient mice (46). Briefly, recipients were treated with the P2X4 inhibitor 5-BDBD (4.25 mg/kg i.p.) or DMSO (vehicle control) 24 h before and immediately after transplantation (53, 54, 57). Donor mice were treated with a single dose of 5-BDBD or DMSO 20 min prior to surgery. Donor mice were anesthetized with ketamine and xylazine (Patterson Veterinary, Devens, MA), intubated and ventilated with isoflurane/oxygen. Lungs were flushed with ice-cold PBS. Left lungs were harvested, and cuffs were placed in the pulmonary artery, pulmonary vein and bronchus. Left lung transplants into recipient mice were performed via a thoracotomy and implantation of the cuffed hilar structures. Peak airway pressures of the transplanted lungs were measured to assess lung function 24 h after transplantation as previously described (58). Transplanted lungs were harvested 24 h after transplantation.

T cell infiltration into lung allografts

T cell recruitment into lung allografts was determined 24 h after transplantation, i.e., at a time before T cell proliferation could affect cell numbers. Lung allografts were digested in 1 mg/ml collagenase D and 1 mg/ml DNAse I (Roche, Sigma-Aldrich) for 1 h at 37°C in a shaking water bath, filtered through a 70 µm cell strainer (Celltreat, Pepperell, MA) and treated with RBC lysis buffer (Biolegend). Cells were treated with anti-mouse CD16/CD32 antibodies (mouse BD Fc block) for 10 min and stained with antibodies against CD3, CD4, CD8 and H-$2K^b$. The number of recipient $CD4^+$ and $CD8^+$ T cells (H-$2K^{b+}CD3^+$) was determined by flow cytometry using Precision Count Beads (Biolegend).

In vitro mixed lymphocyte reactions

Splenocytes were isolated using standard procedures. In vitro mixed lymphocyte reactions were performed in round bottom 96-well plates using $4x10^5$ CellTrace Far Red-labeled C57BL/6 (responder) splenocytes and $6x10^5$ CFSE-labeled, irradiated (10 Gray) BALB/c (stimulator) splenocytes. CCCP and P2 receptor inhibitors were added to the co-cultures for the duration of the experiment as indicated. Proliferation of $CD4^+$ or $CD8^+$ responder T cells was evaluated by flow cytometry after 4 days.

Statistics

Data are shown as mean ± standard deviation (SD) unless otherwise stated. Data were tested for normality with the Shapiro-Wilk test. Differences between normally distributed groups were tested for statistical significance using two-tailed unpaired Student's *t* test or one-way ANOVA followed by post-hoc Holm-Sidak test if two or multiple groups were compared, respectively. Non-parametric Mann-Whitney-U test or Kruskal-Wallis test followed by post-hoc Dunn's test were utilized for two or multiple group comparisons, respectively, when the normality test failed. Pearson's correlation analysis was used to test if parameters were correlated. Differences were considered statistically significant at $p<0.05$.

Study approval

All studies involving human subjects were approved by the Institutional Review Board of Beth Israel Deaconess Medical center and written informed consent was obtained before blood draw. All procedures involving animals were approved by the Institutional Animal Care and Use Committees (AIACUC) of Beth Israel Deaconess Medical Center and Boston Children's Hospital.

Author Contributions

W.G.J. developed the overall study design and supervised the project. C.L. designed, performed and analyzed experiments. K.L. performed lung transplant surgery. T.D., M.A. and M.F. assisted with flow cytometry experiments. Y.K. and C.J.S. provided critical technical assistance. S.D., J.H. and K.K. helped with the analysis of T cell motility data. J.A.L., S.C.R. and G.A.V. provided helpful discussions, provided experimental support, and assisted with the preparation of the manuscript. G.A.V. helped with the design of the lung transplant experiments. C.L and W.G.J. prepared the manuscript with input from the other authors.

Acknowledgements

This work was funded in part by grants from the National Institutes of Health, GM-51477, GM-60475, GM-116162, AI-080582, and T32 GM-103702 (W.G.J.).

Conflict of interest statement

The authors have declared that no conflict of interest exists.

REFERENCES

1. Gerard A, et al. Detection of rare antigen-presenting cells through T cell-intrinsic meandering motility, mediated by Myo1g. *Cell.* 2014;158(3):492-505.
2. Germain RN, Robey EA, and Cahalan MD. A decade of imaging cellular motility and interaction dynamics in the immune system. *Science.* 2012;336(6089):1676-81.
3. Masopust D, and Schenkel JM. The integration of T cell migration, differentiation and function. *Nat Rev Immunol.* 2013;13(5):309-20.
4. Krummel MF, Bartumeus F, and Gerard A. T cell migration, search strategies and mechanisms. *Nat Rev Immunol.* 2016;16(3):193-201.
5. Moreau HD, and Bousso P. Visualizing how T cells collect activation signals in vivo. *Curr Opin Immunol.* 2014;26(56-62.
6. Friedl P, and Weigelin B. Interstitial leukocyte migration and immune function. *Nat Immunol.* 2008;9(9):960-9.
7. Luster AD, Alon R, and von Andrian UH. Immune cell migration in inflammation: present and future therapeutic targets. *Nat Immunol.* 2005;6(12):1182-90.
8. Moreau A, Varey E, Anegon I, and Cuturi MC. Effector mechanisms of rejection. *Cold Spring Harb Perspect Med.* 2013;3(11).
9. Yusen RD, et al. The registry of the International Society for Heart and Lung Transplantation: thirty-first adult lung and heart-lung transplant report--2014; focus theme: retransplantation. *J Heart Lung Transplant.* 2014;33(10):1009-24.
10. Griffith JW, Sokol CL, and Luster AD. Chemokines and chemokine receptors: positioning cells for host defense and immunity. *Annu Rev Immunol.* 2014;32(659-702.
11. Bajenoff M, et al. Stromal cell networks regulate lymphocyte entry, migration, and territoriality in lymph nodes. *Immunity.* 2006;25(6):989-1001.
12. Bleul CC, Fuhlbrigge RC, Casasnovas JM, Aiuti A, and Springer TA. A highly efficacious lymphocyte chemoattractant, stromal cell-derived factor 1 (SDF-1). *J Exp Med.* 1996;184(3):1101-9.
13. Campbell DJ, Kim CH, and Butcher EC. Chemokines in the systemic organization of immunity. *Immunol Rev.* 2003;195(58-71.
14. Gonzalo JA, Lloyd CM, Peled A, Delaney T, Coyle AJ, and Gutierrez-Ramos JC. Critical involvement of the chemotactic axis CXCR4/stromal cell-derived factor-1 alpha in the inflammatory component of allergic airway disease. *J Immunol.* 2000;165(1):499-508.
15. Xu J, et al. Attenuation of obliterative bronchiolitis by a CXCR4 antagonist in the murine heterotopic tracheal transplant model. *J Heart Lung Transplant.* 2008;27(12):1302-10.

16. Burnstock G, and Boeynaems JM. Purinergic signalling and immune cells. *Purinergic Signal.* 2014;10(4):529-64.
17. Cekic C, and Linden J. Purinergic regulation of the immune system. *Nat Rev Immunol.* 2016;16(3):177-92.
18. Junger WG. Immune cell regulation by autocrine purinergic signalling. *Nat Rev Immunol.* 2011;11(3):201-12.
19. Schenk U, et al. Purinergic control of T cell activation by ATP released through pannexin-1 hemichannels. *Sci Signal.* 2008;1(39):ra6.
20. Woehrle T, et al. Pannexin-1 hemichannel-mediated ATP release together with P2X1 and P2X4 receptors regulate T-cell activation at the immune synapse. *Blood.* 2010;116(18):3475-84.
21. Yip L, et al. Autocrine regulation of T-cell activation by ATP release and P2X7 receptors. *FASEB J.* 2009;23(6):1685-93.
22. Gauthier JM, et al. Mechanisms of graft rejection and immune regulation after lung transplant. *Ann Am Thorac Soc.* 2017;14(Supplement_3):S216-S9.
23. Kurishita Y, Kohira T, Ojida A, and Hamachi I. Organelle-localizable fluorescent chemosensors for site-specific multicolor imaging of nucleoside polyphosphate dynamics in living cells. *J Am Chem Soc.* 2012;134(45):18779-89.
24. Ledderose C, Bao Y, Zhang J, and Junger WG. Novel method for real-time monitoring of ATP release reveals multiple phases of autocrine purinergic signalling during immune cell activation. *Acta Physiol (Oxf).* 2015;213(2):334-45.
25. Velasquez S, Malik S, Lutz SE, Scemes E, and Eugenin EA. Pannexin1 channels are required for chemokine-mediated migration of CD4+ T lymphocytes: role in inflammation and experimental autoimmune encephalomyelitis. *J Immunol.* 2016;196(10):4338-47.
26. Ledderose C, et al. Mitochondrial dysfunction, depleted purinergic signaling, and defective T cell vigilance and immune defense. *J Infect Dis.* 2016;213(3):456-64.
27. Ledderose C, et al. Mitochondria are gate-keepers of T cell function by producing the ATP that drives purinergic signaling. *J Biol Chem.* 2014;289(37):25936-45.
28. McCormack JG, Halestrap AP, and Denton RM. Role of calcium ions in regulation of mammalian intramitochondrial metabolism. *Physiol Rev.* 1990;70(2):391-425.
29. Burnstock G, Fredholm BB, North RA, and Verkhratsky A. The birth and postnatal development of purinergic signalling. *Acta Physiol (Oxf).* 2010;199(2):93-147.
30. Coddou C, Yan Z, Obsil T, Huidobro-Toro JP, and Stojilkovic SS. Activation and regulation of purinergic P2X receptor channels. *Pharmacol Rev.* 2011;63(3):641-83.

31. von Kugelgen I, and Hoffmann K. Pharmacology and structure of P2Y receptors. *Neuropharmacology.* 2016;104:50-61.
32. Manohar M, Hirsh MI, Chen Y, Woehrle T, Karande AA, and Junger WG. ATP release and autocrine signaling through P2X4 receptors regulate gammadelta T cell activation. *J Leukoc Biol.* 2012;92(4):787-94.
33. Balázs B, Dankó T, Kovács G, Köles L, Hediger MA, and Zsembery A. Investigation of the inhibitory effects of the benzodiazepine derivative, 5-BDBD on P2X4 purinergic receptors by two complementary methods. *Cell Physiol Biochem.* 2013;32(1):11-24.
34. Abdelrahman A, et al. Characterization of P2X4 receptor agonists and antagonists by calcium influx and radioligand binding studies. *Biochem Pharmacol.* 2017;125:41-54.
35. Jacobson KA, and Müller CE. Medicinal chemistry of adenosine, P2Y and P2X receptors. Neuropharmacology. 2016;104:31-49.
36. Kucia M, et al. CXCR4-SDF-1 signalling, locomotion, chemotaxis and adhesion. *J Mol Histol.* 2004;35(3):233-45.
37. Vicente-Manzanares M, and Sanchez-Madrid F. Role of the cytoskeleton during leukocyte responses. *Nat Rev Immunol.* 2004;4(2):110-22.
38. Campello S, Lacalle RA, Bettella M, Manes S, Scorrano L, and Viola A. Orchestration of lymphocyte chemotaxis by mitochondrial dynamics. *J Exp Med.* 2006;203(13):2879-86.
39. Quantz MA, Bennett LE, Meyer DM, and Novick RJ. Does human leukocyte antigen matching influence the outcome of lung transplantation? An analysis of 3,549 lung transplantations. *J Heart Lung Transplant.* 2000;19(5):473-9.
40. Peltz M, Edwards LB, Jessen ME, Torres F, and Meyer DM. HLA mismatches influence lung transplant recipient survival, bronchiolitis obliterans and rejection: implications for donor lung allocation. *J Heart Lung Transplant.* 2011;30(4):426-34.
41. Sim JA, Broomhead HE, and North RA. Ectodomain lysines and suramin block of P2X1 receptors. *J Biol Chem.* 2008;283(44):29841-6.
42. Bao Y, Chen Y, Ledderose C, Li L, and Junger WG. Pannexin 1 channels link chemoattractant receptor signaling to local excitation and global inhibition responses at the front and back of polarized neutrophils. *J Biol Chem.* 2013;288(31):22650-7.
43. Bao Y, et al. mTOR and differential activation of mitochondria orchestrate neutrophil chemotaxis. *J Cell Biol.* 2015;210(7):1153-64.
44. Chen Y, et al. ATP release guides neutrophil chemotaxis via P2Y2 and A3 receptors. *Science.* 2006;314(5806):1792-5.
45. von Andrian UH, and Mackay CR. T-cell function and migration. Two sides of the same coin. *N Engl J Med.* 2000;343(14):1020-34.

46. Fricke GM, Letendre KA, Moses ME, and Cannon JL. Persistence and adaptation in immunity: T cells balance the extent and thoroughness of search. *PLoS Comput Biol.* 2016;12(3):e1004818.
47. Harris TH, et al. Generalized Levy walks and the role of chemokines in migration of effector CD8+ T cells. *Nature.* 2012;486(7404):545-8.
48. Sato M, et al. Stromal activation and formation of lymphoid-like stroma in chronic lung allograft dysfunction. *Transplantation.* 2011;91(12):1398-405.
49. Babich A, and Burkhardt JK. Coordinate control of cytoskeletal remodeling and calcium mobilization during T-cell activation. *Immunol Rev.* 2013;256(1):80-94.
50. Martin-Cofreces NB, Baixauli F, and Sanchez-Madrid F. Immune synapse: conductor of orchestrated organelle movement. *Trends Cell Biol.* 2014;24(1):61-72.
51. Hancock WW. Chemokine receptor-dependent alloresponses. *Immunol Rev.* 2003;196(37-50.
52. Liu K, et al. Inhibition of the purinergic pathway prolongs mouse lung allograft survival. *Am J Respir Cell Mol Biol.* 2014;51(2):300-10.
53. Barr TP, Hrnjic A, Khodorova A, Sprague JM, and Strichartz GR. Sensitization of cutaneous neuronal purinergic receptors contributes to endothelin-1-induced mechanical hypersensitivity. *Pain.* 2014;155(6):1091-101.
54. Chen H, et al. Effect of P2X4R on airway inflammation and airway remodeling in allergic airway challenge in mice. *Mol Med Rep.* 2016;13(1):697-704.
55. Bosgraaf L, and Van Haastert PJ. Quimp3, an automated pseudopod-tracking algorithm. *Cell Adh Migr.* 2010;4(1):46-55.
56. Campi G, Varma R, and Dustin ML. Actin and agonist MHC-peptide complex-dependent T cell receptor microclusters as scaffolds for signaling. *J Exp Med.* 2005;202(8):1031-6.
57. Casati A, Frascoli M, Traggiai E, Proietti M, Schenk U, and Grassi F. Cell-autonomous regulation of hematopoietic stem cell cycling activity by ATP. *Cell Death Differ.* 2011;18(3):396-404.
58. Liu H, Drew P, Gaugler AC, Cheng Y, and Visner GA. Pirfenidone inhibits lung allograft fibrosis through L-arginine-arginase pathway. *Am J Transplant.* 2005;5(6):1256-63.

Figure 1

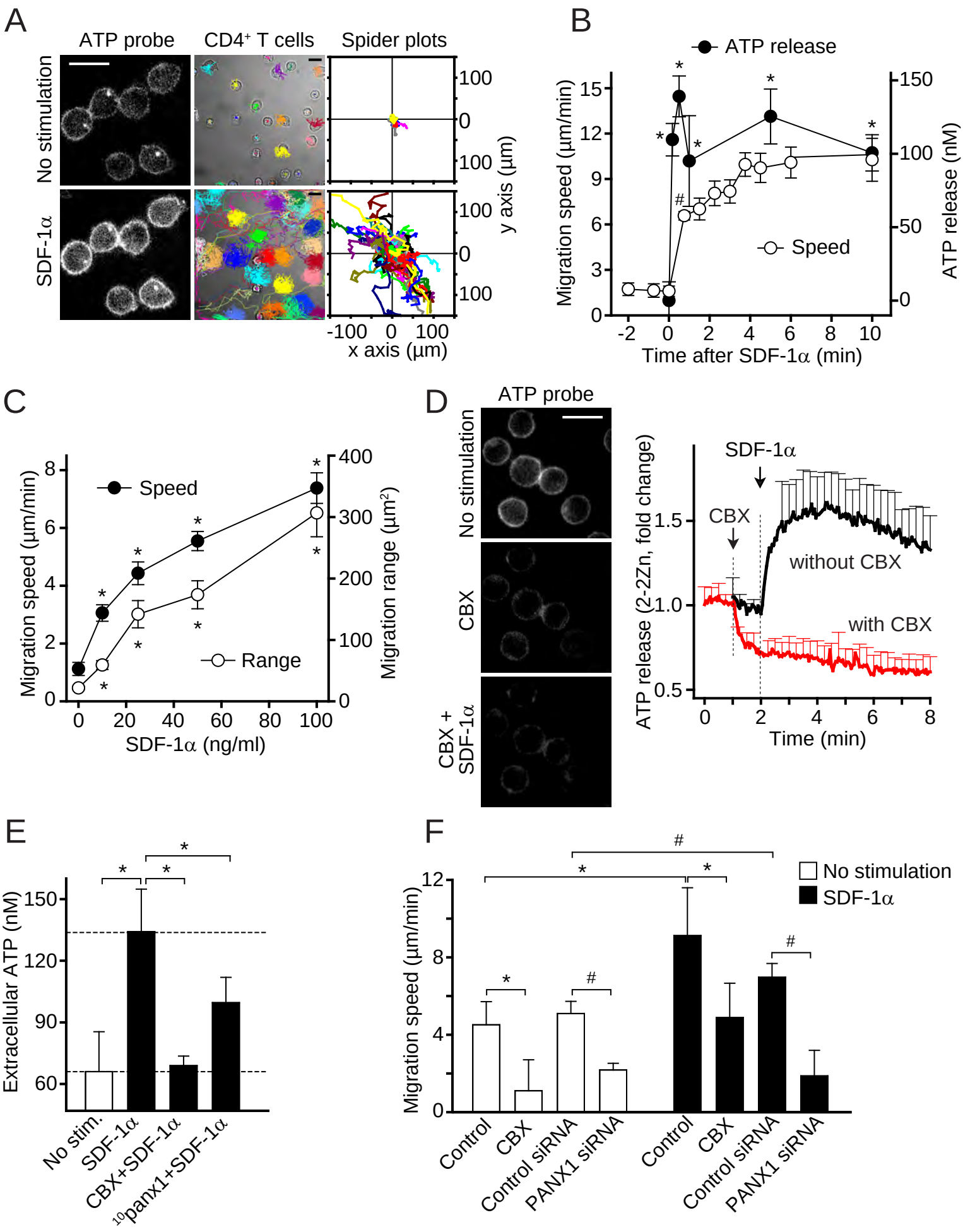
A
ATP probe
CD4⁺ T cells
Spider plots
No stimulation
SDF-1α
100
0
100
y axis (μm)
-100 0 100
x axis (μm)
B
ATP release
Migration speed (μm/min)
ATP release (nM)
Speed
Time after SDF-1α (min)
C
Speed
Range
Migration speed (μm/min)
Migration range (μm²)
SDF-1α (ng/ml)
D
ATP probe
No stimulation
CBX
CBX + SDF-1α
SDF-1α
CBX
without CBX
with CBX
ATP release (2-2Zn, fold change)
Time (min)
E
Extracellular ATP (nM)
No stim.
SDF-1α
CBX+SDF-1α
10panx1+SDF-1α
F
No stimulation
SDF-1α
Migration speed (μm/min)
Control
CBX
Control siRNA
PANX1 siRNA

Figure 1. ATP release through pannexin-1 channels is required for T cell migration.

A ATP release at the cell surface from human $CD4^+$ T cells before and 1 min after stimulation with SDF-1α was visualized with the ATP probe 2-2Zn (left column; 100x objective, scale: 10 µm). Cell migration was tracked for 30 min in the presence or absence of SDF-1α. Paths of individual cells superimposed (center column) or aligned with their origins at x=y=0 (right column) are shown. Data are representative of n=5 experiments. 63x objective; scale: 10 µm (see also video 1). **B** Migration speed and ATP release of $CD4^+$ T cells in response to SDF-1α. **C** Speed and migration range of $CD4^+$ T cells treated with increasing concentrations of SDF-1α (30 min observation). **D** $CD4^+$ T cells were stained with 2-2Zn and the response to CBX (100 µM) or SDF-1α was analyzed with fluorescence microscopy. Representative images before, 0.5 min after addition of CBX and 1 min after addition of SDF-1α (left) and traces (mean ± SD) of n=31 (control) or n=39 (CBX) cells derived from 2 separate experiments are shown. 100x objective; scale: 10 µm (see also video 2). **E** ATP concentrations in the supernatants of $CD4^+$ T cells treated with CBX (50 µM) or ^{10}panx1 (100 µM) and stimulated with SDF-1α for 5 min. **F** Spontaneous or SDF-1α-induced migration speed of Jurkat cells after silencing of PANX1 or treatment with CBX (100 µM; see also video 3). Data in **B** (migration speed), **C** and **F** represent mean ± SD of n=60 cells analyzed in 3 independent experiments. Data in **B** (ATP release) and **E** represent mean ± SD of n=3 independent experiments; **B**, **E**: **p*<0.05 vs. control (one-way ANOVA); #*p*<0.05 (unpaired two-tailed *t* test); **F**: **p*<0.05, #*p*<0.05 (Kruskal-Wallis test).

Figure 2

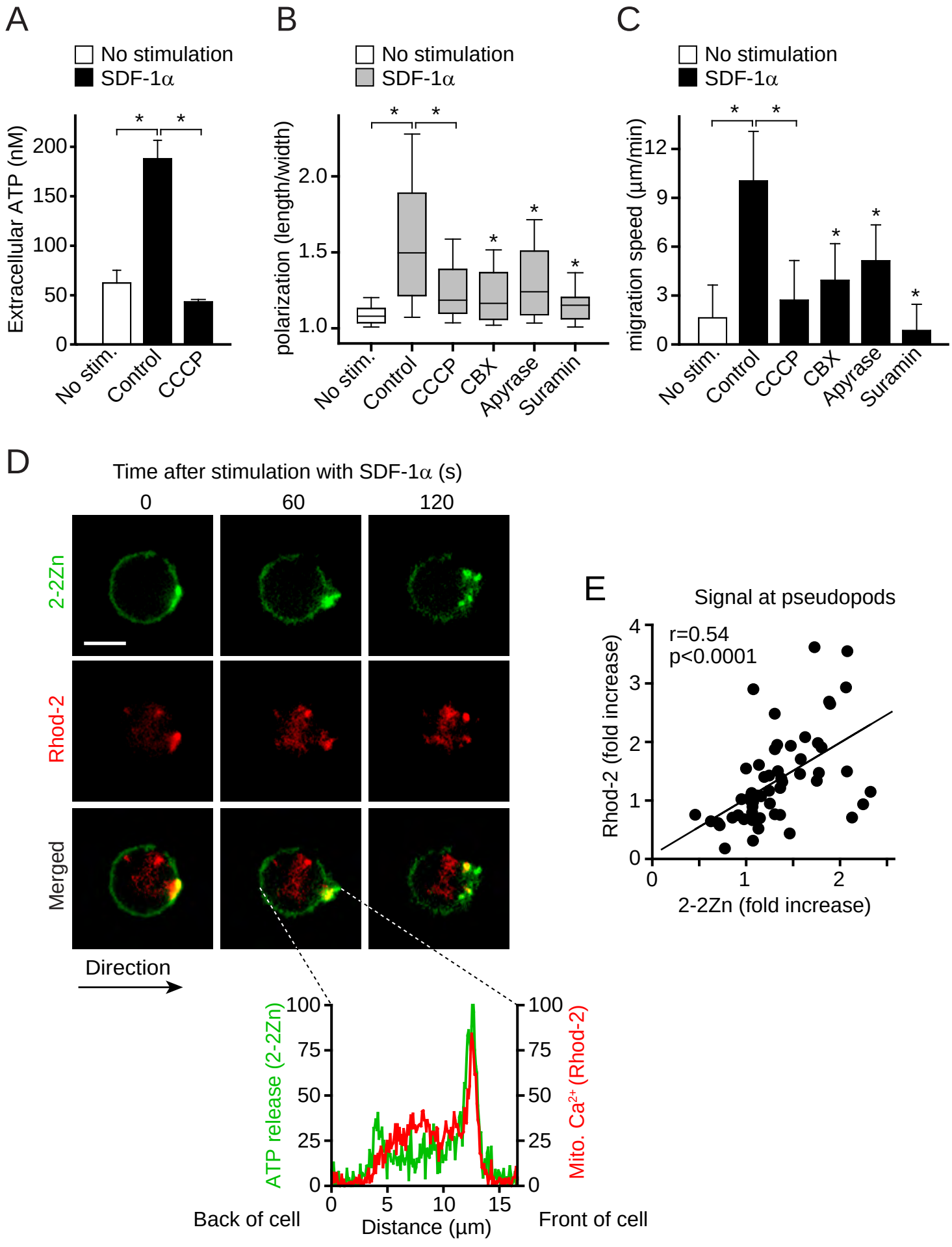
A
No stimulation
SDF-1α
Extracellular ATP (nM)
200
150
100
50
0
*
*
No stim.
Control
CCCP
B
No stimulation
SDF-1α
polarization (length/width)
2.0
1.5
1.0
*
*
*
*
No stim.
Control
CCCP
CBX
Apyrase
Suramin
C
No stimulation
SDF-1α
migration speed (μm/min)
12
9
6
3
0
*
*
*
*
*
No stim.
Control
CCCP
CBX
Apyrase
Suramin
D
Time after stimulation with SDF-1α (s)
0
60
120
2-2Zn
Rhod-2
Merged
Direction
ATP release (2-2Zn)
Mito. Ca2+ (Rhod-2)
100
75
50
25
0
0
5
10
15
Distance (μm)
Back of cell
Front of cell
E
Signal at pseudopods
r=0.54
p<0.0001
Rhod-2 (fold increase)
2-2Zn (fold increase)
4
3
2
1
0
0
1
2

Figure 2. Mitochondria produce the ATP that is released from migrating T cells.

A ATP concentrations were measured in the supernatants of $CD4^+$ T cells treated with CCCP (5 µM) for 10 min and stimulated with SDF-1α for 5 min (mean ± SD, n=3; **p*<0.05 vs. control; one-way ANOVA). **B**-**C** $CD4^+$ T cells were treated with CCCP (5 µM), CBX (50 µM), apyrase (20 U/ml), suramin (100 µM) or cell culture medium (control) for 10 min and polarization (**B**) and migration speed (**C**) in response to SDF-1α were analyzed. Data represent mean ± SD of n=86 (no stimulation), 237 (control), 133 (CCCP), 110 (CBX), 87 (apyrase), and 49 (suramin) cells analyzed in 6 (control) or 3 separate experiments. **p*<0.05 vs. control (Kruskal-Wallis test). **D**-**E** $CD4^+$ T cells were stained with the mitochondrial Ca^{2+} indicator Rhod-2 and the ATP probe 2-2Zn, stimulated with SDF-1α, and ATP release and mitochondrial Ca^{2+} influx were analyzed with fluorescence microscopy (see also video 4). Representative images of 6 individual experiments comprising a total of 55 cells are shown in **D** (scale bar: 5 µm; 100x objective). The histogram shows the distribution of the 2-2Zn and Rhod-2 signal across the cell axis as indicated. **E** 2-2Zn and Rhod-2 fluorescence intensities were measured at the front of polarizing $CD4^+$ T cells and normalized to the fluorescence intensities at the back of the same cell. Data are derived from n=55 cells of 6 individual experiments; r: Pearson's correlation coefficient.

Figure 3

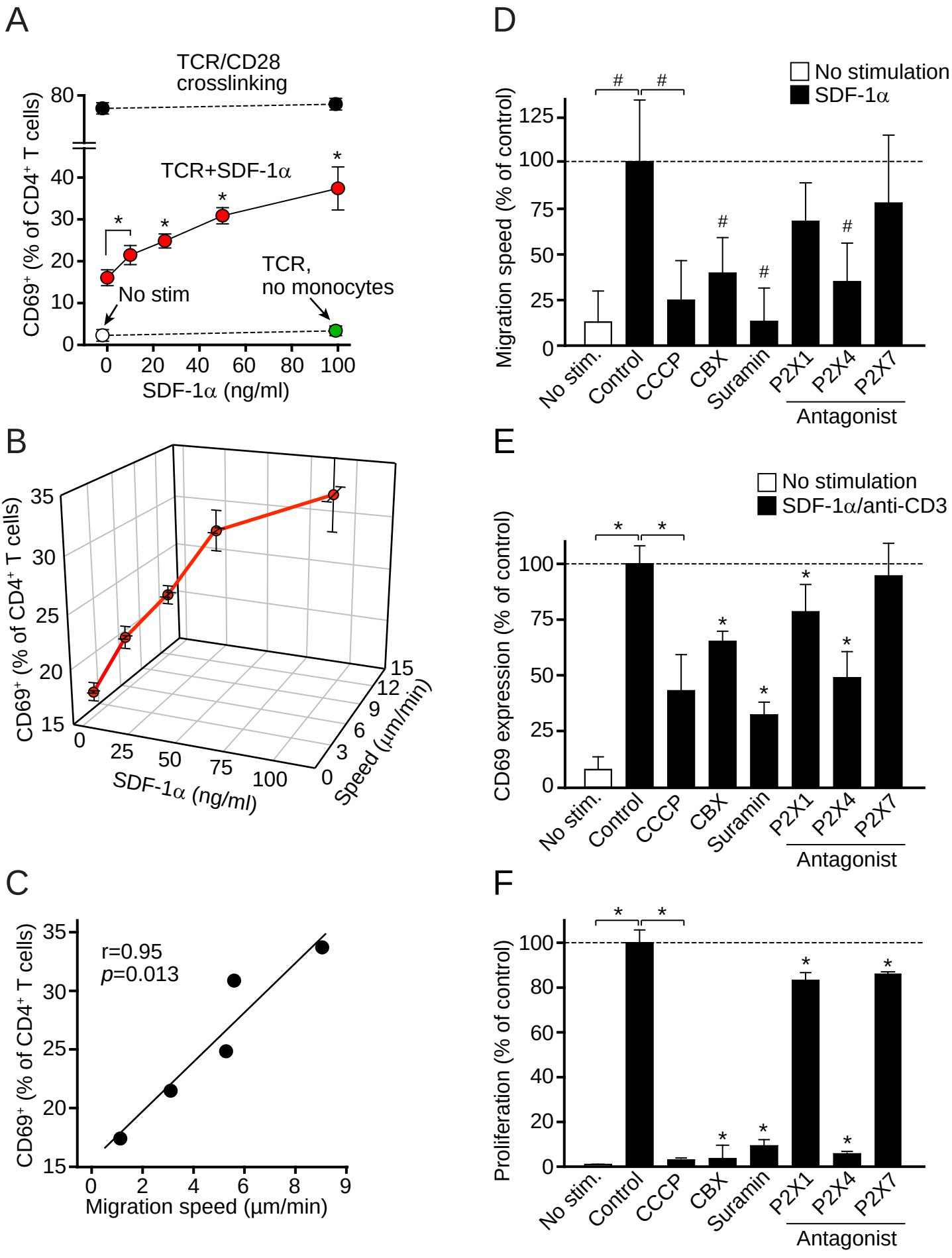
A
TCR/CD28
crosslinking
TCR+SDF-1α
No stim
TCR,
no monocytes
CD69⁺ (% of CD4⁺ T cells)
SDF-1α (ng/ml)
B
CD69⁺ (% of CD4⁺ T cells)
SDF-1α (ng/ml)
Speed (μm/min)
C
r=0.95
p=0.013
CD69⁺ (% of CD4⁺ T cells)
Migration speed (μm/min)
D
No stimulation
SDF-1α
Migration speed (% of control)
No stim.
Control
CCCP
CBX
Suramin
P2X1
P2X4
P2X7
Antagonist
E
No stimulation
SDF-1α/anti-CD3
CD69 expression (% of control)
F
Proliferation (% of control)

Figure 3. T cell migration and activation depends on P2X4 receptors.

A CD69 expression in $CD4^+$ T cells stimulated for 5h with SDF-1α and anti-CD3 antibodies in a PBMC culture was measured by flow cytometry. Positive controls (stimulation with anti-CD3/anti-CD28 coated beads) and negative controls (no stimulation or stimulation with anti-CD3 in monocyte-depleted cultures) were included as indicated. Data represent mean ± SD of n=3 individual experiments. *p<0.05 vs. 0 ng/ml SDF-1α (one-way ANOVA); TCR: T cell receptor. **B** PBMCs were placed into fibronectin-coated glass-bottom chamber slides, stained with APC-labeled anti-CD4 antibodies, stimulated with SDF-1α and migration speed of $CD4^+$ T cells was analyzed by time-lapse microscopy. Data are mean ± SD of n=50 cells analyzed in 3 separate experiments. CD69 expression following stimulation with SDF-1α and anti-CD3 antibodies for 5 h was analyzed as in **A**. Data represent mean ± SD of n=3 separate experiments. **C** Correlation between CD69 expression and migration speed. Data are the mean values of the experiments shown in **B**; r: Pearson's correlation coefficient. **D** $CD4^+$ T cells were treated with CCCP (5 µM), CBX (100 µM), suramin (100 µM), or inhibitors of P2X1 (NF023; 10 µM), P2X4 (5-BDBD; 10 µM), or P2X7 (A438079; 10 µM) receptors and migration speed in response to SDF-1α was analyzed. Data represent mean ± SD of n=80 cells analyzed in n=3 experiments; $^{\#}p$<0.05 vs. control (Kruskal-Wallis test). **E** CD69 expression following TCR stimulation with anti-CD3 for 3h was analyzed as in **A**. **F** Proliferation of $CD4^+$ T cells in a PBMC culture stimulated with anti-CD3 antibodies for 72h was determined by analyzing CFSE dilution. Data in **E** and **F** represent mean ± SD of n=6 (**E**) or n=3 (**F**) individual experiments. *p<0.05 vs. control (one-way ANOVA).

Figure 4

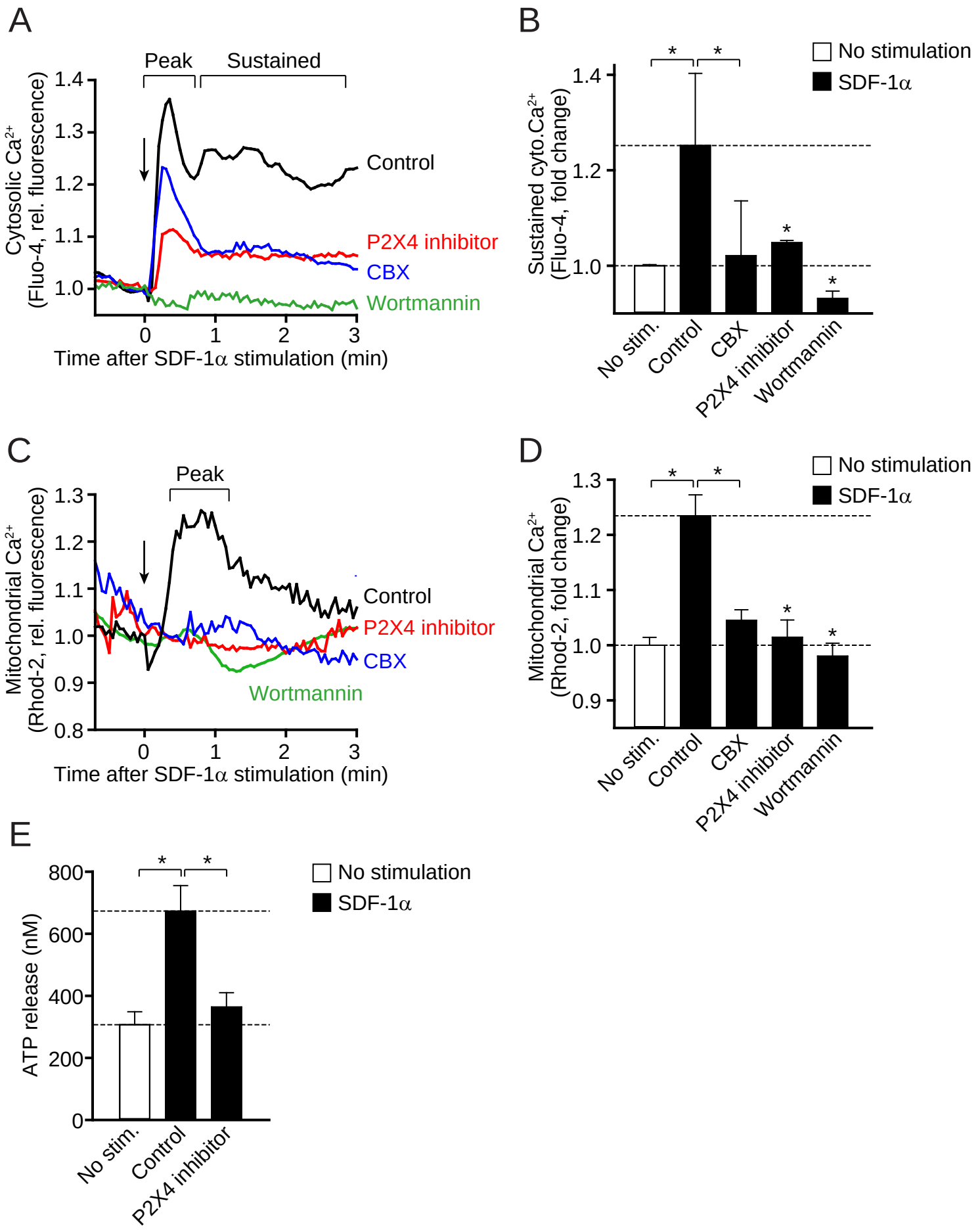
A
Peak
Sustained
Cytosolic Ca2+ (Fluo-4, rel. fluorescence)
1.4
1.3
1.2
1.1
1.0
0
1
2
3
Time after SDF-1α stimulation (min)
Control
P2X4 inhibitor
CBX
Wortmannin
B
No stimulation
SDF-1α
Sustained cyto.Ca2+ (Fluo-4, fold change)
1.4
1.2
1.0
*
No stim.
Control
CBX
P2X4 inhibitor
Wortmannin
C
Peak
Mitochondrial Ca2+ (Rhod-2, rel. fluorescence)
1.3
1.2
1.1
1.0
0.9
0.8
0
1
2
3
Time after SDF-1α stimulation (min)
Control
P2X4 inhibitor
CBX
Wortmannin
D
No stimulation
SDF-1α
Mitochondrial Ca2+ (Rhod-2, fold change)
1.3
1.2
1.1
1.0
0.9
*
No stim.
Control
CBX
P2X4 inhibitor
Wortmannin
E
No stimulation
SDF-1α
ATP release (nM)
800
600
400
200
0
*
No stim.
Control
P2X4 inhibitor

Figure 4. P2X4 receptors regulate Ca^{2+} signaling.

Cytosolic (**A-B**) or mitochondrial (**C-D**) Ca^{2+} levels in $CD4^+$ T cells stimulated in the presence of CBX (50 µM), the P2X4 receptor antagonist 5-BDBD (10 µM) or the PI3K inhibitor wortmannin (10 µM) were recorded by time-lapse fluorescence microscopy. **A** Data are mean Fluo-4 fluorescence traces of n=65 (control), 42 (CBX), 54 (5-BDBD), or 58 (wortmannin) cells from one experiment and are representative of n=3-6 experiments. **B** Averaged plateau fluorescence values ± SD of n=7 (no stimulation), 6 (control), 5 (5-BDBD), or 3 (CBX, wortmannin) separate experiments each comprising averaged data from all cells in a microscopic field (38-71). **C** Data are mean Rhod-2 fluorescence traces of n=32 (control), 31 (CBX), 35 (5-BDBD), or 30 (wortmannin) cells derived from one experiment and are representative of n=3-5 experiments. **D** Averaged peak fluorescence values ± SD of n=5 (no stimulation, control) or 3 (CBX, 5-BDBD, wortmannin) separate experiments each comprising averaged data from all cells in a microscopic field (16-39). **E** Jurkat T cells were treated with 5-BDBD (20 µM) or vehicle control for 10 min. ATP release in response to stimulation with SDF-1α or vehicle control was measured after 5 min (mean ± SD, n=3); *p<0.05 vs. control (one-way ANOVA).

Figure 5

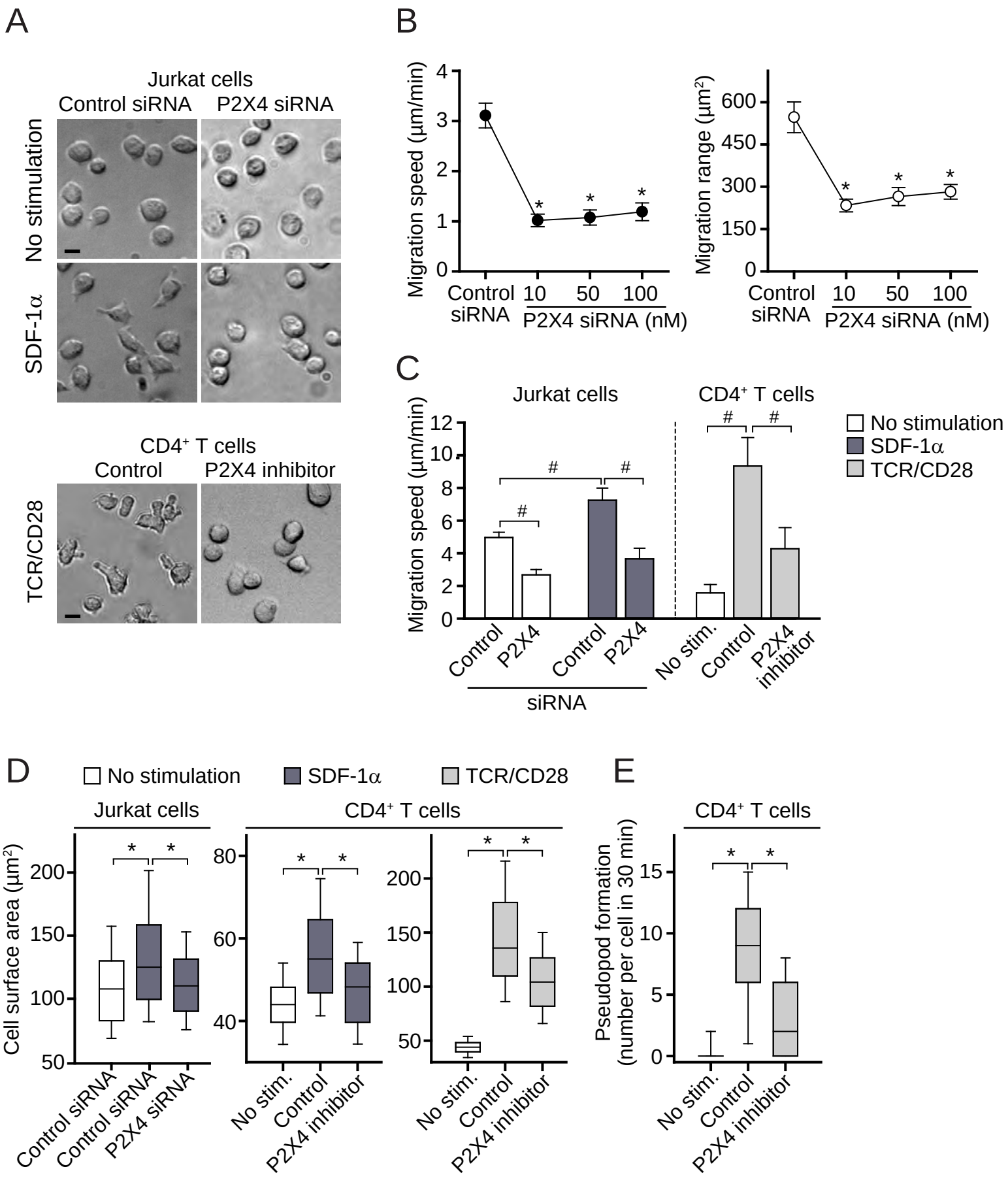
A
Jurkat cells
Control siRNA
P2X4 siRNA
No stimulation
SDF-1α
CD4⁺ T cells
Control
P2X4 inhibitor
TCR/CD28
B
Migration speed (μm/min)
Control siRNA
10
50
100
P2X4 siRNA (nM)
Migration range (μm²)
C
Jurkat cells
CD4⁺ T cells
Migration speed (μm/min)
No stimulation
SDF-1α
TCR/CD28
Control
P2X4
No stim.
P2X4 inhibitor
siRNA
D
Cell surface area (μm²)
Control siRNA
P2X4 siRNA
No stim.
P2X4 inhibitor
E
Pseudopod formation (number per cell in 30 min)

Figure 5. P2X4 receptors regulate T cell polarization, pseudopod formation and migration. **A**-**C** Cell migration after silencing of P2X4 receptors in Jurkat cells or pharmacological P2X4 inhibition (5-BDBD, 10 µM) in $CD4^+$ T lymphoblasts in the presence or absence of SDF-1α. **A** Representative images of n=4 experiments; 20x objective, scale: 10 µm (see also video 6). **B** Jurkat cells were treated with control or P2X4-targeting siRNA at the indicated concentrations and migration speed and range (in 30 min) were analyzed after 48 h. Data represent mean ± SEM of n=60 cells derived from 3 experiments. **C** Jurkat cells were transfected with control or P2X4-targeting siRNA (10 nM) and migration was analyzed after 48 h. Data represent mean ± SD of n=3 (Jurkat cells) or 4 (T cells) separate experiments each comprising 40 cells. **D** Effect of P2X4 silencing or inhibition on the cell surface area of Jurkat cells, primary $CD4^+$ T cells and $CD4^+$ T lymphoblasts stimulated or not with SDF-1α. Box plots show the median and the distribution of n=262, 553, and 276 Jurkat cells, 297, 290, and 127 primary $CD4^+$ T cells, and of 290 control and 127 5-BDBD-treated lymphoblasts. Cells were analyzed in 4 separate experiments. **E** Migration of primary $CD4^+$ T cells (no stimulation) or $CD4^+$ T lymphoblasts treated or not with 5-BDBD was monitored by time-lapse microscopy. The number of pseudopodia formed by a particular cell during the 30 min observation period was recorded. Box plots show the median and the distribution of n=212 (no stimulation), 140 (control), and 82 (5-BDBD) analyzed cells derived from 5 (no stimulation) or 3 independent experiments. *$p<0.05$ vs. control (Kruskal-Wallis test). #$p<0.05$ (one-way ANOVA); TCR: T cell receptor.

Figure 6

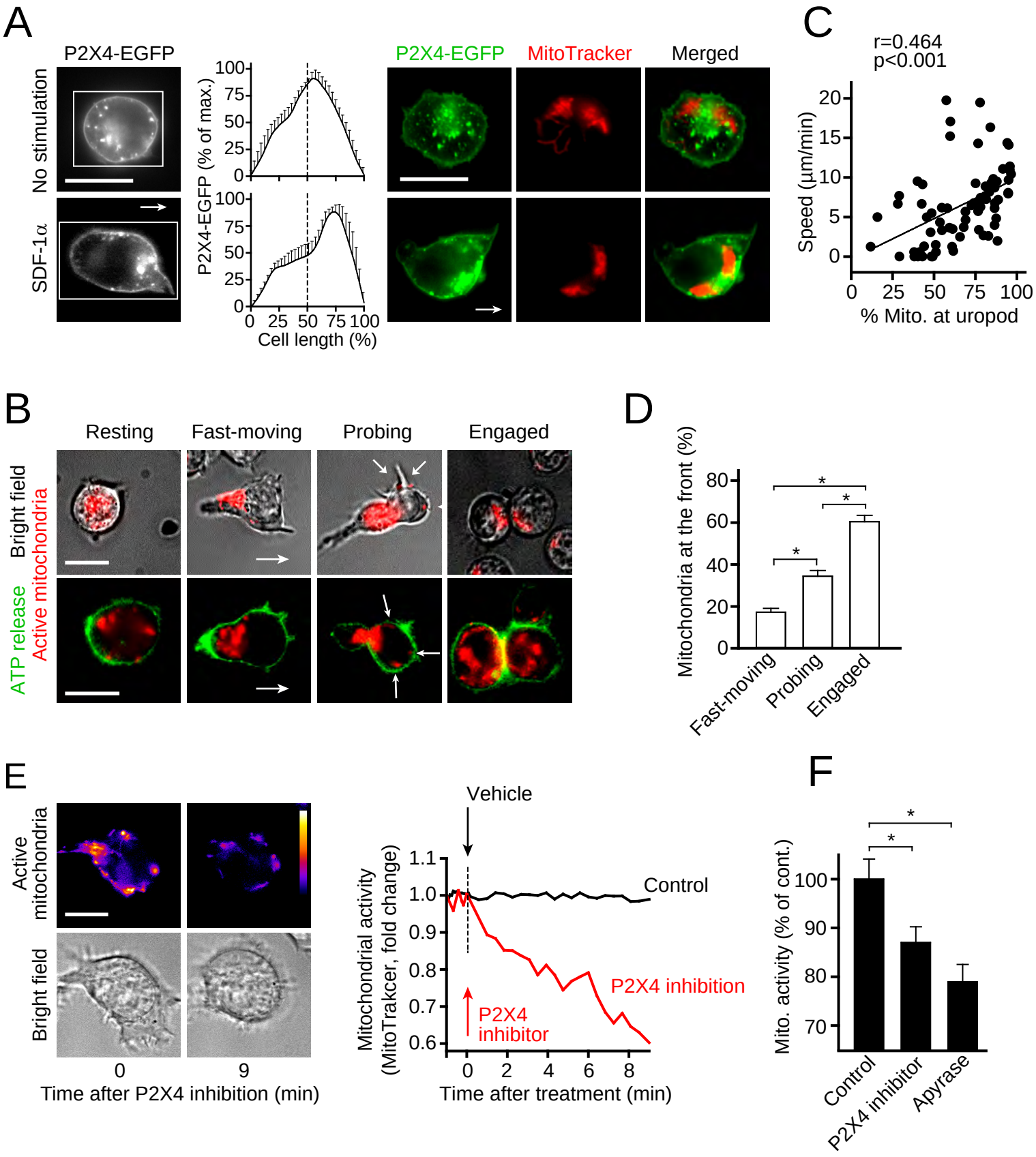
A
P2X4-EGFP
No stimulation
SDF-1α
P2X4-EGFP (% of max.)
Cell length (%)
P2X4-EGFP
MitoTracker
Merged
C
r=0.464
p<0.001
Speed (μm/min)
% Mito. at uropod
B
Resting
Fast-moving
Probing
Engaged
Bright field
Active mitochondria
ATP release
D
Mitochondria at the front (%)
Fast-moving
Probing
Engaged
E
Active mitochondria
Bright field
Time after P2X4 inhibition (min)
Vehicle
Control
P2X4 inhibition
P2X4 inhibitor
Mitochondrial activity (MitoTrakcer, fold change)
Time after treatment (min)
F
Mito. activity (% of cont.)
Control
P2X4 inhibitor
Apyrase

Figure 6. P2X4 receptors promote mitochondrial activation and localized ATP release from migrating T cells.

A Distribution of EGFP-tagged P2X4 receptors and mitochondria in unstimulated and SDF-1α stimulated Jurkat cells. Histograms show the distribution of P2X4 receptor fluorescence along the cell axis as indicated (rectangle) and represent mean ± SD of n=7 independent experiments. 100x objective; arrow: direction of migration (see also video 7). **B** Mitochondria are in the back of fast-moving cells and translocate to the front of cells probing their surroundings or engaging with other cells. $CD4^+$ T lymphoblasts stained with MitoTracker Red CM-H2Xros (top row; 63x objective) or with MitoTracker and 2-2Zn (bottom row; 100x objective) are shown. Images are representative of n=30 (top) or 15 (bottom row) experiments. Arrows in cells probing their environment indicate spots of increased mitochondrial activity (see also video 8). **C** Migration speed and mitochondrial localization were analyzed in 30 s increments in cells derived from 5 different experiments. The results shown comprise n=73 single analyzes; r: Pearson's correlation coefficient. **D** Localization of mitochondria in the front half of fast-moving, probing, or interacting cells. Data represent mean ± SD of n=30 cells, derived from n=7 separate experiments; *p<0.05 (Kruskal-Wallis test). **E** Representative images (left) and fluorescence intensity traces (right) of mitochondrial activity (MitoTracker Red CM-H2Xros) in $CD4^+$ T lymphoblasts before and after P2X4 receptor inhibition (5-BDBD, 10 µM). Color coding was applied to demonstrate differences in mitochondrial activity. Right panel: Change in mitochondrial activity over time following treatment with 5-BDBD or culture medium (control). Data are representative of n=20 cells. 100x objective (see also movie 9). **F** Averaged mitochondrial activity (mean ± SEM) of n=22 (control), n=20 (P2X4 inhibitor), or n=11 (apyrase; 10 U/ml) cells analyzed in 2 (apyrase) or 3 individual experiments; *p<0.05 (one-way ANOVA); scale: 10 µm.

Figure 7

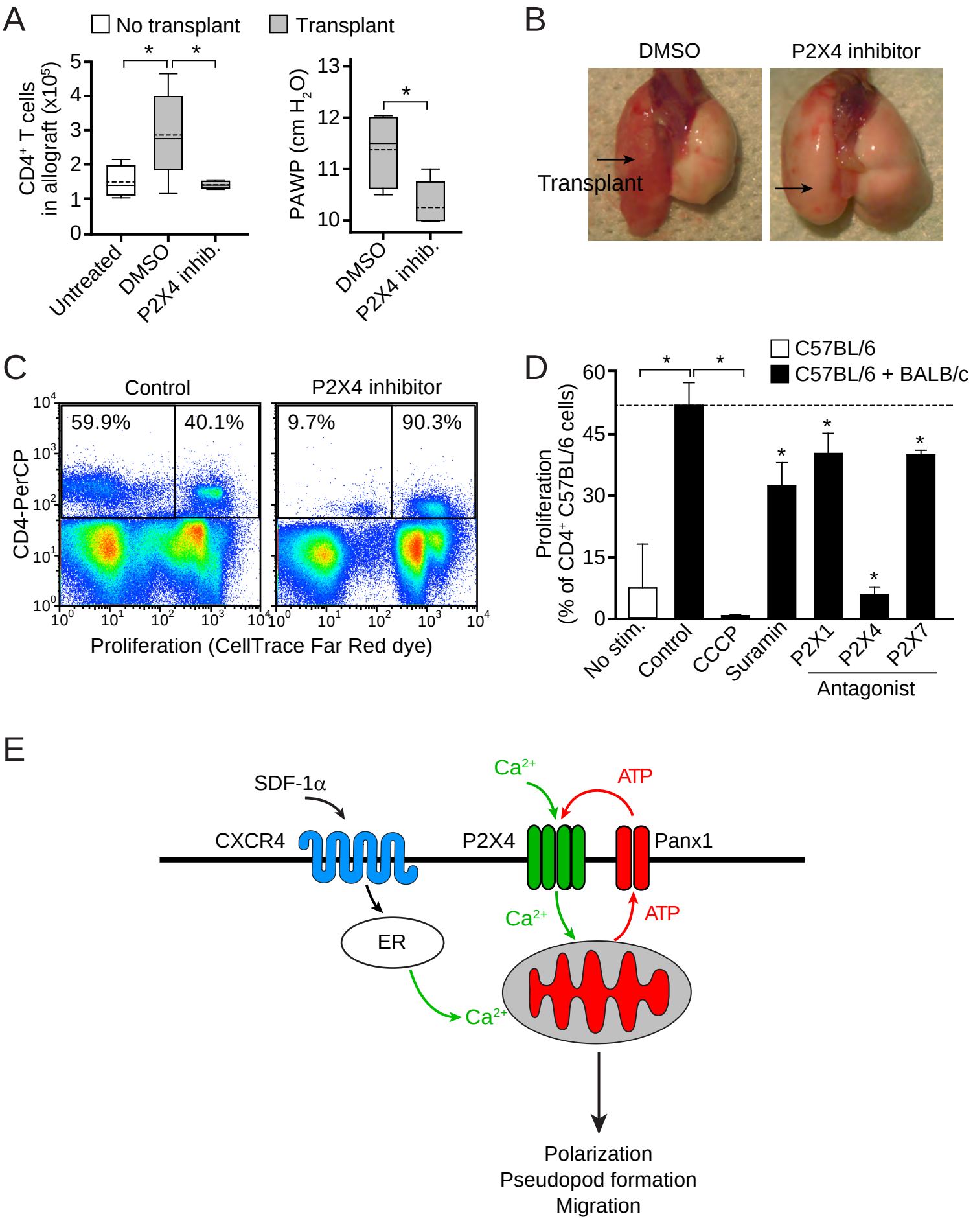
A
No transplant
Transplant
CD4+ T cells in allograft (x10^5)
PAWP (cm H2O)
Untreated
DMSO
P2X4 inhib.
B
DMSO
P2X4 inhibitor
Transplant
C
Control
P2X4 inhibitor
59.9%
40.1%
9.7%
90.3%
CD4-PerCP
Proliferation (CellTrace Far Red dye)
D
C57BL/6
C57BL/6 + BALB/c
Proliferation (% of CD4+ C57BL/6 cells)
No stim.
Control
CCCP
Suramin
P2X1
P2X4
P2X7
Antagonist
E
SDF-1α
CXCR4
P2X4
Panx1
ATP
Ca2+
ER
Polarization
Pseudopod formation
Migration

Figure 7. Inhibition of purinergic signaling prevents T cell recruitment in vivo.

A-**B** Recipient C57BL/6 mice were treated with the P2X4 inhibitor 5-BDBD or vehicle (DMSO) 24 h before and immediately after transplantation of BALB/c lung allografts. **A** The number of $CD4^+$ T cells infiltrating the lung allograft (left) and peak airway pressures (PAWP) in the allograft (right) were measured 24h after transplantation; n=4 (non-transplanted control and P2X4 inhibitor-treated group) or n=6 (DMSO-treated group). Box plots: solid line indicates median, dotted line indicates mean; **p*<0.05, one-way ANOVA (left) or unpaired two-tailed Student's *t* test (right). **B** Representative images of lung allografts 24h after transplantation. **C**-**D** In vitro proliferation of C57BL/6 $CD4^+$ T cells (responders) co-cultured in a mixed lymphocyte reaction with BALB/c splenocytes (stimulators) in the presence or absence of CCCP (1 µM), suramin (100 µM), NF279 (P2X1 antagonist; 20 µM), 5-BDBD (P2X4 antagonist; 20 µM), or A438079 (P2X7 antagonist; 20 µM) for 4 days. Representative dot plots (**C**) and averaged results (mean ± SD; **D**) of n=3 separate experiments are shown; **p*<0.05 vs. control (one-way ANOVA). **E** Purinergic regulation of T cell migration by P2X4 receptors: Chemokine receptors, e.g., CXCR4, trigger the production of ATP by mitochondria, ATP release through PANX1 channels, and autocrine stimulation of P2X4 receptors that facilitate Ca^{2+} influx, sustain mitochondrial ATP production, and promote pseudopod protrusion at the front of cells.